AGU PUBLICATIONS

Geophysical Research Letters

RESEARCH LETTER
10.1002/2015GL065108

Key Points:
- Global body wave coda is not equipartitioned, and the propagation direction is preserved for hours
- Directional equilibration of the wavefield at 40 s period has a mean free time of about 10 h
- Randomization of the teleseismic ambient noise wavefield relies on the distribution of sources

Supporting Information:
- Text S1

Correspondence to:
C. Sens-Schönfelder,
sens-schoenfelder@gfz-potsdam.de

Citation:
Sens-Schönfelder, C., R. Snieder, and S. C. Stähler (2015), The lack of equipartitioning in global body wave coda, *Geophys. Res. Lett.*, *42*, 7483–7489, doi:10.1002/2015GL065108.

Received 26 JUN 2015
Accepted 1 SEP 2015
Accepted article online 7 SEP 2015
Published online 25 SEP 2015

The lack of equipartitioning in global body wave coda

Christoph Sens-Schönfelder[1], Roel Snieder[1,2], and Simon C. Stähler[3,4]

[1]GFZ German Research Centre for Geosciences, Potsdam, Germany, [2]Center for Wave Phenomena, Colorado School of Mines, Golden, Colorado, USA, [3]Ludwig-Maximilians-Universität, München, Germany, [4]Leibniz-Institute for Baltic Sea Research, Rostock, Germany

Abstract Correlation of the coda of large earthquakes can be used to retrieve body waves at teleseismic distances. This retrieval depends on waves propagating with equal energy in all directions (equipartitioning). We carry out a beamforming analysis of body waves at periods of 10 and 40 s recorded at USArray and show that the late coda, up to 10 h after the Okhotsk earthquake, is dominated by waves propagating in the great circle direction; late coda waves are not equipartitioned. This implies for seismic interferometry that teleseismic body waves can only be extracted from the coda when the earthquake and the receivers are located on a great circle. This happens automatically when the employed stations are antipodal or when the autocorrelation of waves is used. The use of long-period ambient seismic noise relies on the distribution of sources because scattering only marginally randomizes directions. This provides insight into recent observations of core phases extracted from seismic interferometry.

1. Introduction

Surface wave studies often rely on the principle of seismic interferometry [*Curtis et al.*, 2006; *Larose et al.*, 2006] to retrieve waves propagating between seismic stations without the dependence on sources such as earthquakes. Seismic interferometry allows for the recovery of the Green's function between arbitrary locations by correlation of a "diffuse" wavefield sensed at those sites. Types of wavefields used for seismic interferometry include thermal fluctuations [*Weaver and Lobkis*, 2001], scattered earthquake coda [*Campillo and Paul*, 2003; *Paul et al.*, 2005; *Tonegawa et al.*, 2009], or ambient seismic noise [*Shapiro and Campillo*, 2004; *Shapiro et al.*, 2005; *Sabra et al.*, 2005]. Theoretically, the prerequisite for convergence toward the Green's function is equipartitioning of the wavefield which refers to an equal distribution of the energy over the available degrees of freedom. *Weaver* [2010] gives a general introduction to the concept of equipartition and discusses the effects of attenuation and open systems that are encountered in seismology. In the context of seismic interferometry it translates into an equilibration of the energy flux over all possible directions and wave types [*Lobkis and Weaver*, 2001; *Snieder et al.*, 2010]. This equilibration can be created by two distinct mechanisms: (1) by a homogeneous distribution of sources or (2) by the propagation in a heterogeneous medium that randomizes directions by scattering and mixes wave types.

In the most common type of applications using ambient seismic noise as source wavefield, it is well known that equipartitioning is often not fulfilled due to an uneven distribution of noise sources [*Stehly et al.*, 2006]. This leads to variations in the recovered amplitudes of direct wave arrivals depending on orientation and location of the station pair and to spurious arrivals resulting from imperfect cancelations of nonphysical amplitudes in the correlation functions [*Snieder et al.*, 2008]. Excitation of the ambient noise by surface sources also leads to an unequal distribution of energy for different wave types strongly favoring surface waves over body waves. The predominance of surface waves in the retrieved waveforms and the difficulty of retrieving body waves by seismic interferometry with ambient noise are due to this lack of equipartitioning of the ambient seismic noise.

To enhance the recovery of body waves, *Tonegawa et al.* [2009] used teleseismic *S* wave coda for cross correlation and obtained direct as well as reflected body waves. Recently, the retrieval of teleseismic body waves from continuous seismic records of several months duration was demonstrated [*Poli et al.*, 2012; *Nishida*, 2013; *Lin et al.*, 2013; *Boué et al.*, 2013]. In these studies networks with dozens of stations were used for stacking to obtain signals of sufficient quality. *Lin and Tsai* [2013] showed that the recovery of teleseismic body waves traveling between antipodal stations is effective for sequences of seismic records that contain large earthquakes.

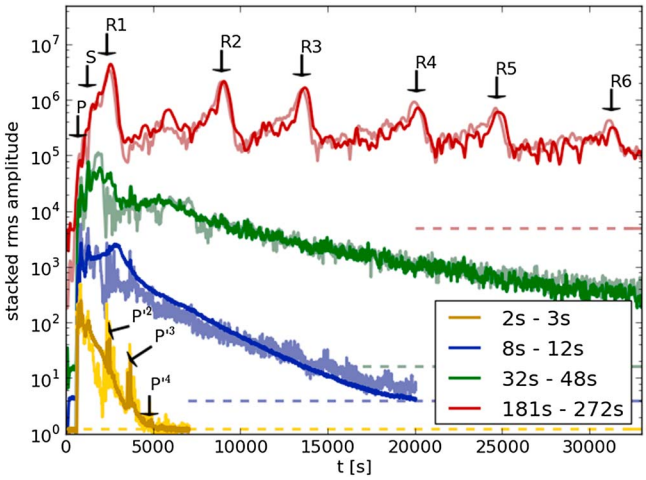

Figure 1. Network-averaged seismogram envelopes in different period bands in comparison with synthetics (pale curves). Envelopes are shifted for clarity. Noise level is indicated by dashed lines. Annotated arrows indicate seismic phases.

This allowed for the retrieval of body waves traversing the Earth between individual stations, which suggests that the nature of the wavefield excited by large earthquakes is better suited for the retrieval of teleseismic body waves than ambient seismic noise.

The retrieval of body waves from earthquake coda requires, however, that the randomization of the wavefield is ensured by scattering at heterogeneities. To first order, heterogeneity of the Earth can be described by a layered 1-D model which does not alter the horizontal propagation direction and slowness of reverberating waves. *Boué et al.* [2014] discuss the role of reverberations for the retrieval of deep phases with seismic interferometry. Additional to the 1-D structure, the Earth contains significant 3-D heterogeneity [*Sato et al.*, 2012], especially in the crust, that should randomize propagation directions to some extent by 3-D scattering.

In this work we investigate globally propagating coda waves of a deep earthquake to study its randomization to assess its suitability for the retrieval of teleseismic body waves with seismic interferometry.

2. The Deep Okhotsk Earthquake

To study the long-period global earthquake coda we analyze the wavefield excited by the 605 km deep M_w8.3 Sea of Okhotsk (west of Kamchatka) earthquake from 24 May 2013 [*GEOFON*, 2013]. This event was the largest earthquake to occur in the mantle transition zone ever recorded [*Ye et al.*, 2013] and thus provides unique possibilities to investigate teleseismic body wave propagation without being obscured by surface waves, which are excited with high energy by shallow earthquakes. We use records of USArray to study the temporal evolution of amplitude and propagation directions of the teleseismic coda wavefield at long lapse times.

Depending on the frequency range, different regimes of scattering are operative. This is illustrated in Figure 1 that shows stacks of envelopes of the USArray stations for different frequency bands. At the highest frequencies (periods between 2 and 3 s) the energy remains above the noise level for about 5000 s and shows clear arrivals of multiply reflected *PKIKP* (P') phases (Figure 1). The presence of ballistic seismic energy that traversed the Earth three or four times (P'^3, P'^4) above the coda level indicates that the path-averaged scattering mean free time for those deeply propagating body waves at this frequency is larger than the absorption time ($t^\star > t_a$). The situation is different in the 8–12 s and 32–48 s period bands where the absence of ballistic arrivals indicates that the wavefield is strongly scattered before it is dissipated ($t^\star < t_a$). For these periods the waves propagate for hours before being damped below the noise level, even though the energy of ballistic waves does not emerge above the level of the smooth envelopes. Surface waves are clearly visible in the lowest frequency band around 200 s period where waves circling the Earth multiple times stand out above the coda for many hours. The reason to limit the display in Figure 1 to this lapse time range is the occurrence of an M_w6.7 aftershock in the sea of Okhotsk 9 h after the main shock.

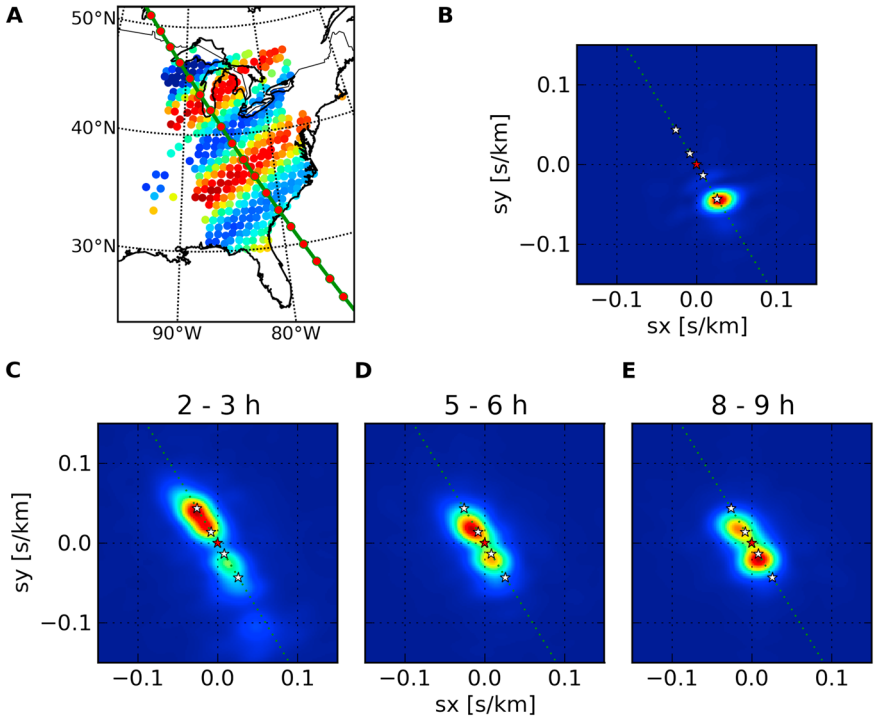

Figure 2. Wavefield across the USArray in the 32–48 s period band. (a) Wavefield at the time of the *P* wave arrival. Line indicates great circle with the source. Distance between dots along the line is 200 km. (b) Energy of the *P* wave arrival as a function of slowness. The width of the peak resembles the response function of the array. (c–e) Slowness maps stacked over time windows 2–3 h, 5–6 h, and 8–9 h, respectively, after the event. Dotted lines in Figures 2b–2e show the direction toward the source. Stars indicate zero slowness (red), direct *P* wave (outer white stars), and $P'P'$ wave (inner white stars).

Envelopes of synthetic waveforms calculated using the spectral-element method AxiSEM *Nissen-Meyer et al.* [2014], details in the supporting information) are shown with pale colors in Figure 1. They demonstrate that the coda decay of the periods above 32 s is well described by preliminary reference Earth model (PREM) [*Dziewonski and Anderson*, 1981]. At higher frequencies, observed envelopes decay faster than predicted by the 1-D model indicating an additional process — most likely 3-D scattering in the heterogeneous crust.

In the following we focus on the 10 s and 40 s period bands where the resolution of the array is most suitable to study the slowness distribution of the wavefield.

3. Composition of the Coda Wavefield

The structure of the coda at intermediate periods indicates that the absorption time is larger than the scattering mean free time. This implies that scattering dominates attenuation. But does this mean that the coda is equipartitioned? To verify this, we investigate the slowness distribution in different frequency bands and lapse time windows. As an illustration of the approach we show the wavefield in the 40 s period band at 900 s lapse time in Figure 2a. The wavefronts are perpendicular to the back azimuth oriented toward the earthquake, and the wavelength of about 800 km indicates a slowness of 0.05 s/km that corresponds to the *P* wave arrival expected at this time. We apply a conventional delay and stack beam forming to the data of the USArray assuming homogeneous velocity within the array. The slowness map (Figure 2b) calculated from a 200 s time interval around the *P* wave arrival shows a clear peak for waves traveling along the great circle with the *P* wave slowness. The peak resembles the array response function.

To investigate the energy propagation in the coda as a function of time, we compute slowness maps for 200 s long time-windows incremented by 100 s over the whole time span of the coda. Stacks of the slowness maps within 1 h windows are shown in Figures 2c–2e. In the 2–3 h lapse time window energy arrives with slownesses less than 0.05 s/km dominantly along the major arc of the great circle (Figure 2c). In later time windows,

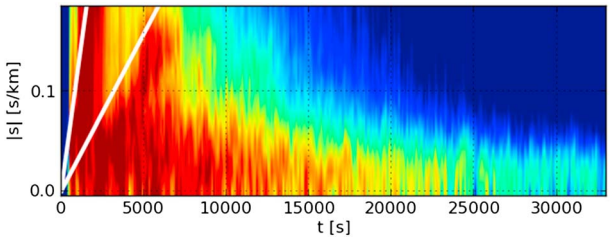

Figure 3. Slowness distribution with time for waves with periods between 32 and 48 s. White lines indicate arrival times of energy that travels along the surface in the shallow Earth. Color scale is logarithmic.

the energy still propagates predominantly along the great circle, but the slowness range narrows. Even after 8 h, energy propagates in the great circle direction, see Figure 2e.

The energy that dominates the slowness maps in Figure 2 arrives with the slowness of body waves with the tendency to decrease over time toward the slowness of core phases. To illustrate this trend, Figure 3 shows the dependence of the energy on the slowness magnitude and time for the 40 s period band. The traveltime-slowness curves for waves traveling along the surface or in the shallow Earth on the minor and major arcs are indicated with white lines. Energy strongly increases to the right of these lines indicating energy propagation along the surface (surface waves or shallow reverberations) also at slownesses above 0.1 s/km. At later lapse times amplitudes at high slownesses decay faster than those of small slownesses thereby narrowing the slowness range of late coda energy. This is in accordance with observations by *Maeda et al.* [2006] at a period of 128 s. The wavefield at late lapse times is dominated by waves propagating in the deep Earth because of the stronger attenuation of seismic waves in the shallow Earth and high Q values in the mantle and core. The superposition of waves propagating in the high Q deep Earth and these shallow propagating waves leaves an imprint on the envelope that has a significant curvature in a logarithmic scale, indicating a combination of different attenuation processes (green curve of Figure 1).

4. Directionality of the Wavefield

The observation of a smooth envelope in Figure 1 at periods above 10 s indicates a randomization of the wavefield because a limited number of ballistic arrivals produce pronounced peaks in the envelope. This appears to be in contrast to the stability of the propagation direction in the plane of the great circle in Figure 2, but both observations together can be explained by reverberations in a layered 1-D structure with sufficient complexity. This has fundamental implications for the Green's function retrieval with seismic interferometry as reverberations do not create secondary sources in the stationary phase regions of station pairs that are not oriented along the great circle with the primary source. However, it is known that heterogeneity in the Earth is 3-D at various length scales. To estimate the imprint of 3-D scattering, we investigate the flux of energy from the great circle into other propagation directions.

As a first step we eliminate energy with slowness above 0.08 s/km that does not correspond to deeply propagating body waves. In the second step we split the slowness maps into four quadrants of which two contain energy that propagates *in* the great circle direction (E_i) and two that contain energy propagation *off* the great circle (E_o) as illustrated in Figure 4a.

To quantify the anisotropy of the wavefield, we set up differential equations for the amount of energy propagating in the two direction ranges:

$$\frac{dE_i}{dt} = \frac{g}{2}(E_o - E_i) - \alpha E_i, \tag{1}$$

$$\frac{dE_o}{dt} = \frac{g}{2}(-E_o + E_i) - \alpha E_o. \tag{2}$$

The energy in the direction of the great circle E_i increases by scattering from E_o into E_i and decreases by scattering from E_i into E_o as described by the term multiplying $g/2$, where g is the coefficient that determines the rate of conversion between E_o and E_i by scattering. The division by 2 accounts for the probability of continuing the propagation in the same azimuthal direction range after scattering. Attenuation is described by the

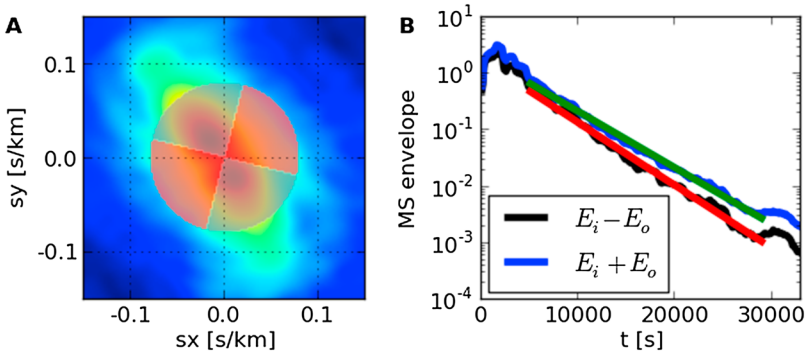

Figure 4. Change of propagation direction. (a) Partitioning of the slowness map into great circle directions (E_i, gray shading) and off great circle directions (E_o, red shading) for slownesses smaller than 0.08 s/km. A stack of the slowness maps from 2–9 h lapse time is in the background in a logarithmic color scale. (b) Sum and difference of the energies E_i and E_o. The slopes fitted in the indicated lapse time ranges are $E_i + E_o \propto \exp(-2.3 \cdot 10^{-4}\ \mathrm{s}^{-1} t)$ and $E_i - E_o \propto \exp(-2.56 \cdot 10^{-4}\ \mathrm{s}^{-1} t)$.

coefficient α that accounts for both intrinsic attenuation and exchange with waves of larger slownesses. The sum and the difference of equations (1) and (2) are

$$\frac{\mathrm{d}(E_i + E_o)}{\mathrm{d}t} = -\alpha(E_i + E_o), \tag{3}$$

$$\frac{\mathrm{d}(E_i - E_o)}{\mathrm{d}t} = -(g + \alpha)(E_i - E_o) \tag{4}$$

and can be integrated to

$$E_i + E_o = e^{-\alpha t}(\bar{E}_i + \bar{E}_o), \tag{5}$$

$$E_i - E_o = e^{-(g+\alpha)t}(\bar{E}_i - \bar{E}_o). \tag{6}$$

$\bar{E}_o$ and $\bar{E}_i$ represent the energies at time $t = 0$. The parameters α and $g + \alpha$ can be determined as the slopes of the curves representing the sum and the difference of E_o and E_i in log scale, respectively (Figure 4b).

At early times the curves for sum and difference are almost identical indicating that all energy is contained in the quadrants propagating in the direction of the great circle ($E_o = 0$). The faster decay of the energy difference compared to the sum indicates that the energy content in both directions converges to an isotropic wavefield ($E_o = E_i$). Using the slopes from Figure 4b, we obtain $\alpha = 0.83\ \mathrm{h}^{-1}$ and $g = 0.094\ \mathrm{h}^{-1}$. This means that the attenuation/leakage time, i.e., the time it takes for the energy to drop by a factor $1/e$ by attenuation and leakage is, 1.2 h. The horizontal transport mean free time, which describes how long the energy propagates before it looses its initial horizontal direction while maintaining the absolute slowness of deep body waves, is about 10.7 h. This indicates weak randomization of propagation directions for small slownesses at a period of 40 s.

At 10 s period the situation is different. After 2 h lapse time the energy is restricted to a small slowness range below 0.03 s/km (Figure 5a). We therefore restrict our analysis to this slowness range. Figure 5b shows E_i and E_o instead of their sum and difference. A superposition of different attenuation mechanisms is reflected in the nonexponential decay of the envelope with time. These distinct attenuation mechanisms become apparent also in the distribution of propagation directions. During the first 2 h lapse time, the energy propagation is almost isotropic as there is no significant difference between the energy propagation in the great circle direction and perpendicular to it. At later times, after 5000 s, the energy contents diverge. A likely explanation is that different wave types with a different degree of directional isotropy and different attenuation are superimposed. One of these wave types is the core phases observed at late lapse times that propagate as *P* energy in a high *Q* deep Earth along the great circle plane with the source. The other constituent that is responsible for the isotropic wavefield before 5000 s lapse time is most likely the locally scattered *S* energy that reverberates in the crust after the arrival of ballistic *S* waves [*Gaebler et al.*, 2015]. This part of the wavefield decays much faster due to the strong attenuation in the crust.

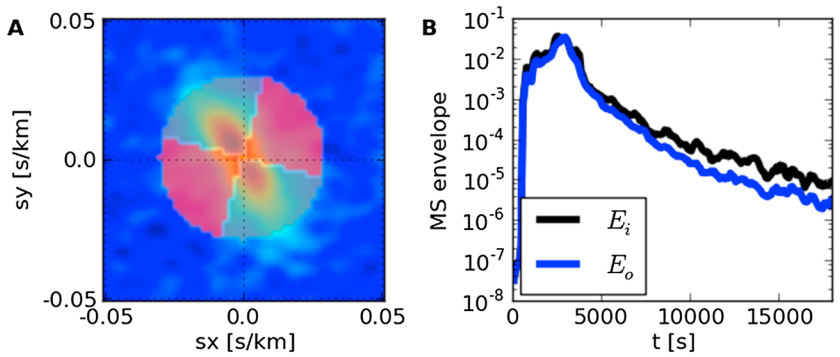

Figure 5. Energy in the in (E_i) and off (E_o) great circle directions for the 8 s–12 s period range. (a) Slowness map stacked from 2–5 h lapse time. (b) Mean square envelopes of E_i and E_o.

5. Discussion

The seismic coda of the 605 km deep teleseismic earthquake in the Sea of Okhotsk shows ballistic surface waves at very long periods (above 100 s) and ballistic body waves at high frequency (above 0.2 Hz). In the intermediate frequency bands around 10 s and 40 s the coda envelopes are smooth and free of ballistic waves. This smooth energy distribution indicates a redistribution of the energy over lapse time. We show that this redistribution is caused predominantly by reverberation in the 1-D-layered structure of the Earth, and that for periods larger than 40 s the wave envelopes are well explained by a 1-D Earth model (PREM). The interaction with the 1-D structure does change neither the ray parameter nor the horizontal direction of propagation. As a result, waves propagate along the great circle and can be identified in the earthquake coda at all the analyzed frequencies even after several hours.

Signatures of 3-D scattering are present at 10 s and 40 s periods, although for the 40 s band this is significant only after a long propagation time. At 10 s and lapse times earlier than 5000 s the wavefield is almost isotropic at all slowness ranges reflecting the strong scattering of *S* energy in the heterogeneous crust. This wavefield is therefore suitable for the retrieval of regional *S* and *P* wave propagation with seismic interferometry [*Tonegawa et al.*, 2009]. At later lapse times the attenuation of shallow *S* waves causes a dominance of deeply propagating *P* wave after 5000 s. These waves interact only weakly with the 3-D heterogeneity and maintain their propagation direction.

At 40 s we do not observe strong crustal scattering, and wave propagation occurs along the great circle also in the early coda and for all slowness ranges. Again, the high slowness component of the wavefield is attenuated first. Analysis of the small slowness range corresponding to core phases makes it possible to quantify the directional randomization of the wavefield. It indicates that the scattering mean free time is approximately 10 h.

For the application of seismic interferometry the persistent dominance of the great circle direction of waves in the coda wavefield has a number of implications: (1) For station pairs that are located on a great circle with the earthquake source, the late coda is well suited to retrieve deeply propagating core phases. (2) Shallow waves may be recovered from the early part of the wavefield. (3) If the station pair is not located on a great circle with the source, the arrival time of retrieved waves is biased resulting in poor recovery of the Green's function [*Boué et al.*, 2014]. (4) Likewise, there is only weak additional randomization of the ambient seismic noise field by scattering at the respective periods that might lead to biased traveltime estimates [*Tsai*, 2009; *Froment et al.*, 2010]. In contrast to the regional wavefield that experiences scattering in the crust, equipartitioning of the globally propagating noise field relies more strongly on the distribution of sources.

There are two special geometric cases in which the influence of the relative positioning of sources and receivers vanishes. First, this is the case of antipodal station pairs. For those stations any source location is on a common great circle; i.e., in the stationary phase region of the receiver pair comprises the whole Earth as the antipodes are caustics [*Snieder and Sens-Schönfelder*, 2015]. The second more important exception is when the autocorrelation is used at a single station [e.g., *Wang et al.*, 2015]. This case is more important as the number of stations is far larger than the number of antipodal station pairs. In this case the late part of coda

of seismic sources is ideally suited to recover the arrival time of reflected phases. Recovery of the full Green's function in any case requires a homogeneous distribution of sources.

Acknowledgments
We thank the Alexander von Humboldt Foundation for the research award that allowed Roel Snieder to be in Potsdam for a sabbatical leave. Data processing was performed using ObsPy [*Krischer et al.*, 2015]. Synthetics were calculated using the spectral-element software *AxiSEM* [*Nissen-Meyer et al.*, 2014] and the *Instaseis* [*van Driel et al.*, 2015] toolbox. The simulation was run at the Leibniz-Rechenzentrum in Garching on the petaflop machine SuperMUC. Data used here were made freely available as part of the EarthScope USArray facility, operated by Incorporated Research Institutions for Seismology (IRIS) and supported by the National Science Foundation, under Cooperative Agreements EAR-1261681.

The Editor thanks Fan-Chi Lin and an anonymous reviewer for their assistance in evaluating this paper.

References

Boué, P., P. Poli, M. Campillo, H. Pedersen, X. Briand, and P. Roux (2013), Teleseismic correlations of ambient seismic noise for deep global imaging of the Earth, *Geophys. J. Int.*, *194*(2), 844–848, doi:10.1093/gji/ggt160.

Boué, P., P. Poli, M. Campillo, and P. Roux (2014), Reverberations, coda waves and ambient noise: Correlations at the global scale and retrieval of the deep phases, *Earth Planet. Sci. Lett.*, *391*, 137–145, doi:10.1016/j.epsl.2014.01.047.

Campillo, M., and A. Paul (2003), Long-range correlations in the diffuse seismic coda, *Science*, *299*(5606), 547–549, doi:10.1126/science.1078551.

Curtis, A., P. Gerstoft, H. Sato, R. Snieder, and K. Wapenaar (2006), Seismic interferometry—Turning noise into signal, *Leading Edge*, *25*(9), 1082–1092, doi:10.1190/1.2349814.

Dziewonski, A. M., and D. L. Anderson (1981), Preliminary reference Earth model, *Phys. Earth. Planet. Inter.*, *25*(4), 297–356, doi:10.1016/0031-9201(81)90046-7.

Froment, B., M. Campillo, P. Roux, P. Gouédard, A. Verdel, and R. L. Weaver (2010), Estimation of the effect of nonisotropically distributed energy on the apparent arrival time in correlations, *Geophysics*, *75*(5), SA85–SA93, doi:10.1190/1.3483102.

Gaebler, P. J., C. Sens-Schönfelder, and M. Korn (2015), The influence of crustal scattering on translational and rotational motions in regional and teleseismic coda waves, *Geophys. J. Int.*, *201*, 355–371, doi:10.1093/gji/ggv006.

GEOFON (2013), M_w 8.3 earthquake, Sea of Okhotsk, 2013-05-24 (moment tensor solution), doi:10.5880/GEOFON.gfz2013kbsi.

Krischer, L., T. Megies, R. Barsch, M. Beyreuther, T. Lecocq, C. Caudron, and J. Wassermann (2015), ObsPy: A bridge for seismology into the scientific Python ecosystem, *Comput. Sci. Discovery*, *8*(1), 1–17, doi:10.1088/1749-4699/8/1/014003.

Larose, E., L. Margerin, A. Derode, B. van Tiggelen, M. Campillo, N. Shapiro, A. Paul, L. Stehly, and M. Tanter (2006), Correlation of random wavefields: An interdisciplinary review, *Geophysics*, *71*(4), SI11–SI21, doi:10.1190/1.2213356.

Lin, F.-C., and V. C. Tsai (2013), Seismic interferometry with antipodal station pairs, *Geophys. Res. Lett.*, *40*, 4609–4613, doi:10.1002/grl.50907.

Lin, F.-C., V. C. Tsai, B. Schmandt, Z. Duputel, and Z. Zhan (2013), Extracting seismic core phases with array interferometry, *Geophys. Res. Lett.*, *40*, 1049–1053, doi:10.1002/grl.50237.

Lobkis, O., and R. Weaver (2001), On the emergence of the Green's function in the correlations of a diffuse field, *J. Acoust. Soc. Am.*, *110*, 3011–3017.

Maeda, T., H. Sato, and M. Ohtake (2006), Constituents of vertical-component coda waves at long periods, *Pure Appl. Geophys.*, *163*(2–3), 549–566, doi:10.1007/s00024-005-0031-9.

Nishida, K. (2013), Global propagation of body waves revealed by cross-correlation analysis of seismic hum, *Geophys. Res. Lett.*, *40*, 1691–1696, doi:10.1002/grl.50269.

Nissen-Meyer, T., M. van Driel, S. C. Stähler, K. Hosseini, S. Hempel, L. Auer, A. Colombi, and A. Fournier (2014), AxiSEM: Broadband 3-D seismic wavefields in axisymmetric media, *Solid Earth*, *5*(1), 425–445, doi:10.5194/se-5-425-2014.

Paul, A., M. Campillo, L. Margerin, E. Larose, and A. Derode (2005), Empirical synthesis of time-asymmetrical Green functions from the correlation of coda waves, *J. Geophys. Res.*, *110*, B08302, doi:10.1029/2004JB003521.

Poli, P., M. Campillo, and H. Pedersen (2012), Body-wave imaging of Earth's mantle discontinuities from ambient seismic noise, *Science*, *338*(6110), 1063–1065, doi:10.1126/science.1228194.

Sabra, K. G., P. Gerstoft, P. Roux, W. A. Kuperman, and M. C. Fehler (2005), Surface wave tomography from microseisms in Southern California, *Geophys. Res. Lett.*, *32*, L14311, doi:10.1029/2005GL023155.

Sato, H., M. Fehler, and T. Maeda (2012), *Seismic Wave Propagation and Scattering in the Heterogeneous Earth*, 2nd ed., 494 pp., Springer, Berlin.

Shapiro, N. M., and M. Campillo (2004), Emergence of broadband Rayleigh waves from correlations of the ambient seismic noise, *Gephys. Res. Lett o.*, *31*, L07614, doi:10.1029/2004GL019491.

Shapiro, N. M., M. Campillo, L. Stehly, and M. H. Ritzwoller (2005), High-resolution surface-wave tomography from ambient seismic noise, *Science*, *307*(5715), 1615–1618.

Snieder, R., and C. Sens-Schönfelder (2015), Seismic interferometry and stationary phase at caustics, *J. Geophys. Res. Solid Earth*, *120*, 4333–4343, doi:10.1002/2014JB011792.

Snieder, R., K. van Wijk, M. Haney, and R. Calvert (2008), Cancellation of spurious arrivals in Green's function extraction and the generalized optical theorem, *Phys. Rev. E*, *78*(3), 36606, doi:10.1103/PhysRevE.78.036606.

Snieder, R., Y. Fan, E. Slob, and K. Wapenaar (2010), Equipartitioning is not sufficient for Green's function extraction, *Earthquake Sci.*, *23*, 403–415.

Stehly, L., M. Campillo, and N. M. Shapiro (2006), A study of the seismic noise from its long-range correlation properties, *J. Geophys. Res.*, *111*, B10306, doi:10.1029/2005JB004237.

Tonegawa, T., K. Nishida, T. Watanabe, and K. Shiomi (2009), Seismic interferometry of teleseicmic *S*-wave coda for retrieval of body waves: An application to the Philippine Sea slab underneath the Japanese Islands, *Geophys. J. Int.*, *178*(3), 1574–1586, doi:10.1111/j.1365-246X.2009.04249.x.

Tsai, V. C. (2009), *On Establishing the Accuracy of Noise Tomography Travel-Time Measurements in a Realistic Medium*, vol. 178, 1555–1564.

van Driel, M., L. Krischer, S. C. Stähler, K. Hosseini, and T. Nissen-Meyer (2015), Instaseis: Instant global seismograms based on a broadband waveform database, *Solid Earth*, *6*(2), 701–717, doi:10.5194/se-6-701-2015.

Wang, T., X. Song, and H. H. Xia (2015), Equatorial anisotropy in the inner part of Earth's inner core from autocorrelation of earthquake coda, *Nat. Geosci.*, *8*(3), 224–227, doi:10.1038/NGEO2354.

Weaver, R. L. (2010), Equipartition and retrieval of Green's function, *Earthquake Sci.*, *23*(5), 397–402, doi:10.1007/s11589-010-0738-2.

Weaver, R. L., and O. I. Lobkis (2001), Ultrasonics without a source: Thermal fluctuation correlations at MHz frequencies, *Phys. Rev. Lett.*, *87*, 134301, doi:10.1103/PhysRevLett.87.134301.

Ye, L., T. Lay, H. Kanamori, and K. D. Koper (2013), Energy release of the 2013 M_w 8.3 Sea of Okhotsk earthquake and deep slab stress heterogeneity, *Science*, *341*(6152), 1380–1384, doi:10.1126/science.1242032.